The holocephalan ratfish endoskeleton shares trabecular and areolar mineralization patterns, but not tesserae, with elasmobranchs little skate and catshark, and appears paedomorphic

Oghenevwogaga J. Atake[1], Fidji Berio[2], Melanie Debiais-Thibaud[2], B. Frank Eames[1]

[1]Department of Anatomy, Physiology, and Pharmacology, University of Saskatchewan, Saskatoon, Canada

[2] Institut des Sciences de l'Evolution, University of Montpellier, CNRS, IRD, EPHE, Montpellier, France

Correspondence

B. F. Eames,

2D01-107 Wiggins Rd, Saskatoon, SK, S7N 5E5 Canada

Tel: +1 (306)966-6534

Email: b.frank@usask.ca

Website: https://www.eameslab.ca/

Abstract

Specific character traits of mineralized endoskeletal tissues need to be clearly defined and comprehensively examined among extant chondrichthyans (elasmobranchs, such as sharks and skates, and holocephalans, such as chimaeras) to understand their evolution. For example, tiles of mineralized polygonal structures called tesserae occur at cartilage surfaces in chondrichthyans, but recent studies showing trabecular mineralization at elasmobranch cartilage surfaces suggest that tesserae are not as common as previously thought. Also, while areolar mineralized tissue in elasmobranchs is generally considered a unique, shared chondrichthyan feature, some chondrichthyan species demonstrate bone-like tissues in both a specific region of tesserae termed the cap zone and continuous (not tiled) mineralized neural arches. To clarify the distribution of specific endoskeletal features among extant chondrichthyans, adult skeletal tissues in a holocephalan chimaera (spotted ratfish) and two elasmobranchs (small-spotted catshark and little skate) were characterized using synchrotron radiation and desktop micro-CT imaging, and histological and immunofluorescent assays. Endoskeletal mineralization in the ratfish, catshark, and little skate varied both quantitively in tissue mineral density (TMD), and qualitatively in the morphology and localization of mineralized structures and tissues. For example, TMD of several skeletal elements was significantly lower in ratfish, compared to catshark and little skate. Trabecular and areolar mineralization were shared among these extant chondrichthyan species, but tesserae and bone-like tissues were not. Interestingly, three separate analyses argued that the chimaera endoskeleton retains embryonic features (i.e., paedomorphic with respect to elasmobranchs). This study further proposes general terminology for character states of the extant

chondrichthyan endoskeleton and infers those states in ancestral chondrichthyans with reference to fossil data.

Key words: chondrichthyan endoskeleton, mineralization patterns, sharks, skates, chimaeras, tesserae, trabecular, areolar, bone-like tissues, paedomorphism

Introduction

The skeleton of chondrichthyans, or cartilaginous fishes, has long fascinated evolutionary biologists (Daniel, 1934; Janvier, 1996; Kölliker, 1860; Maisey, 2013; Ørvig, 1951; Smith and Hall, 1990; Wurmbach, 1932). However, only in the past two decades has an active research community revealed the histological and molecular complexity of extant chondrichthyan skeletal tissues. Even so, these studies are limited in scope, focussing mostly on specific skeletal features of the Elasmobranchii subclass of extant Chondrichthyes, such as sharks, skates, and rays (Atake et al., 2019; Dean et al., 2017; Eames et al., 2007; Johanson et al., 2012; Kemp and Westrin, 1979; Omelon et al., 2014; Porter et al., 2006; Seidel et al., 2016), with only a few including the Holocephali subclass, such as chimaera (Gillis et al., 2011; Herbert et al., 2022; Pears et al., 2020; Seidel et al., 2020; Smith et al., 2020). Unfortunately, an in-depth description of the extant holocephalan endoskeleton is lacking, leading to a deficit in understanding skeletal tissue character states across extant chondrichthyans.

Like most vertebrates, skeletal mineralization in extant chondrichthyans occurs by incorporation of biominerals into extracellular compartments of skeletal tissues (Golub, 2009; Lowenstam, 1981; Omelon et al., 2014), giving rise to diverse mineralized tissue types in several anatomical sites of the chondrichthyan endoskeleton. Traditionally recognized as a defining endoskeletal feature of Chondrichthyes, tesserae form a mineralization pattern consisting of an array of distinct, polygonal units at the surface of cartilages (Kemp and Westrin, 1979; Maisey, 2013; Maisey et al., 2021). In skates, however, a recently characterized trabecular mineralization pattern lies directly underneath the polygonal pattern of tesserae (Atake et al., 2019). In fact, the cartilage surface in several endoskeletal regions of skates and rays only

contains the trabecular mineralization pattern (Atake et al., 2019; Jayasankar et al., 2020), suggesting that polygonal tesserae may not be as common as traditionally thought. Like polygonal tesserae, the little skate trabecular mineralization also forms an arrayed pattern, but the repeating units are in the form of trabecular struts interspersed by unmineralized regions, leading us to call them trabecular tesserae (Atake et al., 2019; Atake and Eames, 2021). Descriptions of a trabecular mineralization pattern in the endoskeleton of sharks or chimaeras are currently lacking, leaving open the possibility that this is a phenotype specific to the Batoidea superorder (including skates and rays) of the subclass Elasmobranchii. In some chimaeras, the surfaces of cartilage in the anterior fused vertebrae (synarcual) and chondrocranium have sheets of mineralization that abut one another (Pears et al., 2020; Seidel et al., 2020), but these do not have an arrayed pattern of repeating units, so perhaps they should not be called tesserae.

Recent evidence suggests that histological features of tesserae may vary according to the mineralization pattern. Traditional polygonal tesserae have distinct histological zones, with a cap zone superficial to a body zone near the surface of chondrichthyan cartilage (Atake et al., 2019; Berio et al., 2021; Kemp and Westrin, 1979; Seidel et al., 2016). While skates have polygonal tesserae, trabecular tesserae in little skate have very small or even absent cap zones overlying extensive body zones (Atake et al., 2019). Additionally, specific regions of tesserae termed spokes are hypermineralized and often devoid of cells, and spokes appear to be a common feature of tesserae regardless of their mineralization pattern (Atake et al., 2019; Pears et al., 2020; Seidel et al., 2020; Seidel et al., 2016). Careful 3D spatial analyses are needed to correlate histological zones and mineralization patterns of tesserae.

92 Some chondrichthyans have mineralized endoskeletal tissues that have been
93 characterized as bone-like (Atake and Eames, 2021). For example, the cap zone of tesserae
94 displays bony features, like elongate cell lacunae in a mineralized ECM of densely packed type I
95 collagen (Col1) fibers (Atake et al., 2019; Kemp and Westrin, 1979; Seidel et al., 2017; Seidel et
96 al., 2016). Unlike the cap zone, the body zone displays typical features of hyaline cartilage,
97 which is the main cartilage type in vertebrates (Goldring et al., 2006). The body zone consists of
98 round chondrocyte lacunae embedded in a mineralized matrix abundant in loosely packed type
99 II collagen (Col2) fibers and sulfated glycosaminoglycans (Enault et al., 2015; Seidel et al., 2017).
100 As another example of bone-like tissue, several elasmobranch species have a non-tiled,
101 mineralized perichondral tissue in their neural arches (Atake et al., 2019; Berio et al., 2021;
102 Bordat, 1987; Eames et al., 2007; Kemp and Westrin, 1979; Seidel et al., 2016). The neural arch
103 bone-like tissue demonstrates morphological and histological features of perichondral bone,
104 including a compact mineralization pattern, elongate cell lacunae, canaliculi-like channels
105 connecting adjacent lacunae, and tightly packed Col1 fibers (Bordat, 1987; Eames et al., 2007;
106 Kemp and Westrin, 1979; Peignoux-Deville et al., 1982; Rossert and de Crombrugghe, 2002;
107 Seidel et al., 2017). Bone-like tissues might be a defining feature of extant chondrichthyans, but
108 relevant data from chimaeras are needed.

109 Finally, areolar mineralized tissue is generally considered a unique feature of the extant
110 chondrichthyan endoskeleton, characterized mostly in elasmobranchs as large sheets of
111 mineralization in the notochordal sheath of the vertebral body (centrum) (Didier, 1995;
112 Ridewood and MacBride, 1921). Areolar mineralized tissue typically contains concentric
113 lamellae of elongate lacunae in a fibrocartilage-like extracellular matrix and a compact

114 mineralization pattern (Atake et al., 2019; Criswell et al., 2017; Dean and Summers, 2006;
115 Eames et al., 2007). Mineralized centra are not thought to be common in chimaeras, but when
116 present, they can appear as multiple mineralized rings in each vertebral segment, which
117 contrasts with the grossly biconcave morphology of segmented centra in elasmobranchs
118 (Gadow and Abbott, 1895).

119 With hopes of revealing shared and clade-specific features among chondrichthyans,
120 here we clarify many of the unresolved issues highlighted above, proposing specific terminology
121 for character states of the extant chondrichthyan endoskeleton (Table 1). Testing the
122 hypothesis that extant chondrichthyans share histological and morphological features of
123 endoskeletal mineralized tissues, adult tissues in several endoskeletal regions of the spotted
124 ratfish *Hydrolagus colliei* (chimaera), small-spotted catshark *Scyliorhinus canicula* (shark), and
125 little skate *Leucoraja erinacea* (skate) were characterized using synchrotron radiation and
126 desktop micro-CT imaging, and histological and immunofluorescent assays. Tesseral
127 mineralization, cap zones, and neural arch bone-like tissues were absent in the ratfish, but
128 present in these elasmobranchs, and three separate analyses argued that this chimaera displays
129 skeletal paedomorphosis, or retention of embryonic features (Garstang, 1922; Liem, 2001).
130 While additional chondrichthyan species can bolster these findings, the data argue that
131 trabecular and areolar mineralization patterns, but not tesserae, are shared among extant
132 chondrichthyans. Considering fossil outgroups, we finish by inferring ancestral and derived
133 character states of the chondrichthyan endoskeleton.

134

135 Table 1. Character states of the mineralized chondrichthyan endoskeleton

Character	**State**	**Description**
mineralization pattern	polygonal tesserae	array of distinct polygonal units between the perichondrium and trabecular tesserae
	trabecular tesserae	array of distinct trabecular struts, often with hypermineralized spokes, below the perichondrium
	non-tesseral trabeculae	non-arrayed, distinct trabecular struts, often with hypermineralized spokes, below the perichondrium
	areolar	compact sheets or rings in the notochordal sheath
	bone-like tissue	compact regions between the perichondrium and a cartilaginous core in neural arches and cap zones
histological feature	body zone	distinct region of mineralized tissue below the perichondrium, containing Col2, rounded cell lacunae, and low-cellularity spokes
	cap zone	distinct region of mineralized tissue between the perichondrium and body zone, containing densely-packed Col1 fibers and elongated cell lacunae

	bone-like tissue	mineralized tissue of densely-packed Col1 fibres and elongated cell lacunae connected by canaliculi-like channels

Results

Adult mineralized tissues in spotted ratfish had lower tissue mineral density (TMD) than small-spotted catshark or little skate

To assess whether chimaeras demonstrate skeletal mineralization in anatomical sites that are homologous to those of elasmobranchs, 3D rendering of micro-CT images of anterior regions of adult ratfish were qualitatively and quantitatively analyzed (Fig. 1A,B). Micro-CT images revealed mineralized tissues in several endoskeletal regions, including neural arches and centra of segmented vertebrae (Fig. 1C,D), skeletal elements in the pharyngeal skeleton (Fig. 1E), and the fused vertebral synarcual (Fig. 1F,G). Although elasmobranchs mineralize neural arches in their precaudal and caudal vertebrae (Atake et al., 2019; Berio et al., 2021; Eames et al., 2007), mineralized neural arches were present mainly in precaudal vertebrae of ratfish (Fig. 1C,D; data not shown). Mineralized skeletal elements in the pharyngeal skeleton included the basihyal, Meckel's, ceratohyal, basibranchial, hypobranchials, and ceratobranchial (Fig. 1E). Spinal nerve foramina are common in the synarcual of cartilaginous fishes and were present in the ventral sides of the ratfish synarcual (Fig. 1F; Claeson, 2011; Johanson et al., 2015; Pears et al., 2020). Unlike the synarcual in skates and other batoids, where mineralized centra are not discernible (Atake et al., 2019; Claeson, 2011), the synarcual in ratfish had distinct mineralized centra (Fig. 1G).

155 TMDs of the synarcual, neural arches, and centra in ratfish, catshark, and little skate
156 were quantitated and compared, where possible, since sharks do not have a synarcual (Fig. 1H).
157 Because little skate does not have centra within the synarcual, centra in the ratfish synarcual
158 were digitally segmented and excluded for synarcual TMD data. The average TMD of the ratfish
159 synarcual was 0.31± 0.11 gHA/cm^3, significantly lower than the TMD of the little skate
160 synarcual, which was 0.94 ± 0.04 gHA/cm^3 (Fig. 1H; p= 6.5x10^{-4}). Similarly, the TMD of ratfish
161 neural arches (0.40 ± 0.05 gHA/cm^3) was significantly lower than the TMD of neural arches of
162 either catshark (0.81 ± 0.04 gHA/cm^3; p=9 x10^{-6}) or little skate (0.96 ± 0.04 gHA/cm^3; p=4.5x10^{-7};
163 Fig. 1H). The average TMD of ratfish centra (0.42 ± 0.10 gHA/cm^3) was also significantly lower
164 than the TMD of centra of either catshark (0.84 ± 0.02 gHA/cm^3; p=1.1 x10^{-4}) or little skate (0.88
165 ± 0.05 gHA/cm^3; p=3.4 x10^{-5}; Fig. 1H). In ratfish, TMD of segmented centra within the synarcual
166 was similar to that of centra in segmented vertebrae (0.46 ± 0.11 gHA/cm^3). These analyses
167 showed that the synarcual, neural arches, and centra in ratfish had significantly lower TMDs
168 compared to homologous elements in catshark and little skate.
169

170 **Neural arches in ratfish lacked bone-like tissue**

171 To clarify whether chimaeras have bone-like tissue like elasmobranchs, micro-CT and
172 histological analyses of neural arches in segmented precaudal vertebrae of ratfish were
173 compared to neural arches in segmented precaudal vertebrae of catshark and little skate.
174 Mineralization of neural arches in ratfish was organized in a non-continuous pattern of small
175 compact and trabecular regions (Fig. 2A). This mineralization pattern in spotted ratfish
176 contrasted with the continuous mineralization pattern displayed by the compact, bone-like

177 tissue in catshark and little skate (Fig. 2B,C; Atake et al., 2019; Berio et al., 2021). Furthermore,
178 cross-section views demonstrated that mineralized tissues in ratfish were restricted to the
179 medial and lateral periphery of the neural arches (Fig. 2D). By contrast, mineralization of bone-
180 like tissues in catshark and little skate extended much deeper in the neural arch (Fig. 2E,F).

181 Histologically, Alizarin red staining of calcium showed that mineralized tissues in ratfish
182 neural arches were much thinner and not continuous like bone-like tissues in catshark and little
183 skate neural arches (Fig. 2G-I). Alcian blue staining of sulfated proteoglycans marked cartilage in
184 most neural arch regions in ratfish, while only the cartilaginous core regions of catshark and
185 little skate neural arches were Alcian blue-positive (Fig. 2G-I). The neural arch core in catshark
186 was mostly unmineralized cartilage, while that of little skate was mineralized cartilage (Fig.
187 2H,I). Birefringence of picrosirius-stained, tightly packed collagen fibers (likely reticular) were
188 observed in muscles lateral to neural arches in all three species (Fig. 2J-L). Birefringence was not
189 observed in ratfish neural arches, whereas birefringence in neural arch bone-like tissues was
190 observed in catshark and little skate (Fig. 2K,L). Most regions (including unmineralized cartilage
191 and mineralized tissue) in ratfish neural arches demonstrated Col2 immunofluorescence (Fig.
192 2J). Only the cartilaginous core in neural arches of catshark and little skate demonstrated Col2
193 immunofluorescence (Fig. 2K,L). These results showed that bone-like tissue was absent in
194 neural arches of ratfish, and the non-continuous pattern of mineralized tissue in ratfish neural
195 arches was mineralized cartilage.

196

197 **Novel characterization of non-tesseral trabecular mineralization in ratfish and catshark**
198 **showed the absence of a bone-like cap zone**

To clarify whether tesserae are defining endoskeletal features of extant chondrichthyans, morphological patterns and histological features of mineralized tissues were characterized in ceratohyals of ratfish, caudal vertebrae of catshark, and precaudal vertebrae and hyomandibulae of little skate. Desktop micro-CT renderings of ratfish ceratohyals and catshark haemal arches revealed mineralized tissues with a trabecular pattern like that of trabecular tesserae in the vertebral neural spine of little skate (Fig. 3A-G). However, the trabecular pattern in ratfish and catshark was not as clearly organized into arrays of repeating trabecular units like that of trabecular tesserae in little skate, and for this reason, trabecular patterns in ratfish and catshark were characterized as non-tesseral. In the hyomandibulae and other skeletal elements of little skate, a trabecular mineralization pattern occurred underneath the superficial polygonal tesseral pattern (Fig. 3D,H,H'; Atake et al., 2019). Notably, many regions in ratfish (vertebrae, pharyngeal skeleton, and the synarcual) and catshark (vertebrae and ceratohyals) did not exhibit the polygonal mineralization pattern typical of tesserae (Atake et al., 2019; Kemp and Westrin, 1979; Maisey, 2013; Marramà et al., 2019; Seidel et al., 2016; Wilga and Ferry, 2015).

To assess whether trabecular mineralized tissues in ratfish, catshark, and little skate exhibit similar histological features, cross sections of tissues with non-tesseral patterns were compared to those with tesseral patterns. Non-tesseral mineralized tissues in Alcian blue-positive perichondral regions in ratfish ceratohyals and catshark haemal arches stained with Alizarin red (Fig. 3I,J; perichondrium marked by straight dashed line). The discrete organization of mineralized tissues and Alcian blue and Alizarin red staining patterns of non-tesseral mineralized tissues in ratfish and catshark were similar to the tesseral body zone in little skate

221 (Fig. 3I-L). However, Alcian blue-positive cartilage separated Alizarin red-positive non-tesseral
222 mineralized tissues from overlying perichondrium in ratfish and catshark (Fig. 3I,J). A bone-like
223 cap zone just below the perichondrium was only present in tesseral mineralized tissues in little
224 skate (Fig. 3K,L; perichondrium marked by straight dashed line). The bone-like cap zone stained
225 more intensely than the body zone with Alizarin red and was relatively smaller and larger in
226 trabecular tesserae and polygonal tesserae, respectively (Fig. 3K,L). Perichondrium of both non-
227 tesseral and tesseral mineralized tissues stained with the general connective tissue dye fast
228 green (Fig. 3M-P). Matrix of the little skate bone-like cap zone was fast green-positive and had
229 birefringent collagen fibers, but these staining patterns were not observed in non-tesseral
230 mineralized tissues in ratfish and catshark (Fig. 3M-T). Instead, regions just below the
231 perichondrium of ratfish ceratohyals and catshark haemal arches stained for sulfated
232 proteoglycans by Safranin O and were Col2-positive cartilage (Fig. 3M,N,Q,R). Staining patterns
233 of non-tesseral mineralized tissues in ratfish and catshark were generally consistent with those
234 of mineralized cartilage in the tesseral body zone of little skate, although chondrocyte lacunae
235 in these regions were not obvious in ratfish (Fig. 3I-T). Therefore, histological features of
236 trabecular mineralized tissues in ratfish ceratohyals and catshark haemal arches were similar to
237 only the body zones of tesserae in little skate, which consisted of mineralized cartilage.
238

239 **Spatial organization of histological features correlated with trabecular and polygonal**
240 **mineralization patterns**

241 Given that trabecular mineralized tissues typically have small or even absent cap zones,
242 and polygonal tesserae typically have large cap zones, histology and micro-CT segmentation

243 were used to see whether there was a correlation between histological features and
244 mineralization patterns in ratfish and little skate. After demineralization, non-tesseral tissues in
245 ratfish and tesseral tissues in little skate exhibited spokes, which are regions of very low
246 cellularity in the body zone that often appeared as tears or sectioning artifacts and did not stain
247 strongly with any Trichrome dye (Fig. 4A-C). Non-spoke regions of the body zone stained either
248 slightly blue for collagen fibers with Trichrome's aniline blue or magenta with Trichrome's acid
249 fuchsin, and these staining patterns were consistent in non-tesseral and tesseral tissues.
250 Tightly-wound collagen fibers were marked by Trichrome's acid fuchsin, but only in the larger
251 and smaller cap zones of little skate polygonal and trabecular tesserae, respectively (Fig. 4A-C).
252 Also, the presence of elongate lacunae distinguished the cap zone from other tesseral regions
253 (Fig. 4A-C).

254 Enough histological features were also visible in synchrotron radiation micro-CT
255 renderings (Fig. 4D-F), making it possible to segment and analyze the spatial correlation
256 between mineralization patterns and histological features, such as cap zone and spokes (red
257 and blue, respectively, in Fig. 4G-I). Segmentation of 3D renderings of deep surface views
258 showed that hypermineralized spokes were localized to non-tesseral and tesseral trabecular
259 mineralization patterns in ratfish and little skate, respectively (blue in Fig. 4J-L). Unlike the well-
260 organized spokes seen in trabecular patterns of little skate tesserae, spokes in ratfish trabecular
261 mineralized tissues were patchy and less-organized. Therefore, both non-tesseral and tesseral
262 trabecular mineralization patterns correlated with, and appeared to derive from, spokes and
263 non-spoke regions within body zones.

Unlike little skate polygonal tesserae, trabecular mineralized tissues in ratfish and trabecular tesserae in skate both displayed identical trabecular mineralization patterns whether viewed from the superficial or deep surfaces of the cartilage (Fig. 4J,K,M,N). The smaller cap zones in trabecular tesserae were discernible on the superficial surface, but they were not as laterally extensive as cap zones of polygonal tesserae (Fig. 4H,I,N,O). Thus, larger and laterally extensive cap zones appeared to be the reason why polygonal tesserae displayed a superficial polygonal mineralization pattern.

Ratfish centra contained areolar mineralized tissue

To clarify whether ratfish, catshark, and little skate have areolar mineralized tissue, morphological and histological features of centra were revealed by desktop micro-CT and section histology. Precaudal vertebrae in ratfish had multiple rings of centra per vertebral segment (i.e., unit with paired neural arches and basidorsals; Fig. 5A). Each centrum in ratfish precaudal vertebrae demonstrated a compact mineralization pattern like that of centra in the catshark and little skate (Fig. 5A-C). However, no ratfish centrum displayed the typical biconcave gross morphology associated with elasmobranch centra (Fig. 5A-C; (Atake et al., 2019; Clement, 1992; Criswell et al., 2017).

Alizarin red and Alcian blue section histology showed that centra in ratfish, catshark, and little skate comprised of compact mineralized tissue spanning different numbers of centrum layers. The ratfish centrum only had mineralized tissue in the middle layer, but an outer layer of the catshark centrum had mineralized cartilage, while inner and outer layers of the little skate centrum contained mineralized cartilage (Fig. 5D-I). Areolar mineralized tissues

286 in the middle layer of the centrum of ratfish, catshark, and little skate had elongate cell lacunae
287 organized in concentric lamellae (inserts in Fig. 5G-I; Atake et al., 2019; Criswell et al., 2017;
288 Eames et al., 2007), and they were birefringent (data not shown). Markers of cartilage differed
289 in areolar mineralized tissue among ratfish, catshark, and little skate (Fig. 5J-O). In ratfish,
290 areolar mineralized tissue had relatively strong Safranin O staining and Col2
291 immunofluorescence (Fig. 5J,M). Areolar mineralized tissue in catshark demonstrated weak
292 Safranin O staining and Col2 immunofluorescence (Fig. 5K,N). By contrast, areolar mineralized
293 tissue in little skate did not display Safranin O staining or Col2 immunofluorescence (Fig. 5L,O).
294 Overall, these data suggested that ratfish have areolar mineralized tissue.
295

296 **Qualitative and quantitative features of centra in the adult ratfish were similar to those of**
297 **little skate embryos**

298 The biconcave centra morphology is thought to be acquired in elasmobranchs during
299 development when the perichordal sheath becomes constricted by mesenchymal cells (Arratia
300 et al., 2001; Gadow and Abbott, 1895; Kölliker, 1860). To shed light on differences in adult
301 centra morphology, morphological and histological features of centra in a developmental series
302 of little skate were compared to those of adult ratfish. In little skate embryos and juveniles,
303 desktop micro-CT renderings showed mineralization in the centrum and pairs of neural arches,
304 basidorsals, and haemal arches of each vertebral segment (Fig. 6A-C). Expanding upon recent
305 work showing that anterior and posterior segments of somites fuse during skate vertebral
306 development, similar to tetrapods (Criswell and Gillis, 2020), independent anterior and
307 posterior mineralizations of each interneural appeared to later fuse during development. In

308 adult ratfish, each vertebral segment of paired neural arches and basidorsals had an average of
309 six centra (Fig. 6D). Digital segmentation of synchrotron radiation (SR) micro-CT renderings
310 showed that centra in little skate stage 32 embryos were slightly constricted in the middle of
311 each element's anterior-posterior axis, and this constriction progressed through 6.5 cm disc
312 width (DW) juveniles, when the classic biconcave morphology was present (Fig. 6E-G). SR micro-
313 CT renderings showed that adult ratfish centra were constricted to a similar extent as younger
314 centra in little skate embryos (Fig. 6E,F,H). In little skate embryos, Alcian blue and Alizarin red
315 section histology showed that the areolar mineralized tissue initiated in the middle layer of the
316 centrum and had elongate cell lacunae organized in concentric lamellae, similar to that
317 observed in adult ratfish (Fig. 5D; Fig. 6I,J). At later developmental stages of little skate, such as
318 6.5 cm DW juveniles, the outer layer of the centrum also demonstrated mineralized cartilage
319 (Fig. 6K).

320 To further confirm these morphological and histological similarities of centra in little
321 skate embryos and adult ratfish, TMDs of centra in the developmental series of little skate were
322 compared to that of adult ratfish. TMD of little skate centra increased significantly from stage
323 32 to stage 33 embryos (p= 9.5 x10^{-3}), while TMD of 6.5 cm DW juveniles was only significantly
324 higher than TMD of stage 32 embryos (Fig. 6L; p=9.6 x10^{-4}). TMD of adult ratfish centra was
325 significantly higher than TMD of centra in little skate stage 32 embryos, but it was statistically
326 indistinguishable from TMD of centra in little skate stage 33 embryos and 6.5 cm DW juveniles
327 (Fig. 6L). Therefore, adult ratfish centra had morphological, histological, and TMD similarities
328 with centra from little skate embryos, particularly those at stage 33.

329

Discussion

Which tissues are common in the extant chondrichthyan endoskeleton? Bone-like and areolar tissues have been characterized in several members of the chondrichthyan subclass Elasmobranchii, such as sharks, skates, and rays (Atake et al., 2019; Berio et al., 2021; Bordat, 1987; Kemp and Westrin, 1979; Ørvig, 1951; Peignoux-Deville et al., 1982; Seidel et al., 2016). In addition, polygonal tesserae are traditionally associated with chondrichthyans (Atake et al., 2019; Kemp and Westrin, 1979; Maisey, 2013; Marramà et al., 2019; Seidel et al., 2016; Wilga and Ferry, 2015), but trabecular tesserae were recently characterized in skates and rays (Atake et al., 2019; Jayasankar et al., 2020).

Two main qualities of this paper go a long way in revealing features of the ancestral chondrichthyan endoskeleton. First, we clearly identifed discrete character states of extant chondrichthyan endoskeletons (Table 1), helping to unify terminology of important features for the growing chondrichthyan research community. Second, we presented extensive, side-by-side comparative data across various extant chondrichthyans, two elasmobranch species (small-spotted catshark and little skate) and one chimaera/holocephalan (spotted ratfish). Including ratfish is another critical aspect of this paper, because holocephalans are generally understudied, but must be considered when inferring ancestral chondrichthyan traits. Importantly, previous characterization of skeletal mineralization in other adult chimaeridae neither focused on segmented neural arches to analyze bone-like tissues or areolar mineralization, nor clarified histological zones of tesserae (Berio et al., 2021; Debiais-Thibaud, 2018; Pears et al., 2020; Seidel et al., 2020)

Our and other published data across various extant and fossil chondrichthyan species can be compiled to compare character states of the extant endoskeleton and infer the ancestral condition (Fig. 7). In what appears to be a novel character trait of crown chondrichthyans, trabecular mineralization occurs in many endoskeletal regions in several elasmobranch and chimaera species, including some fossil chondrichthyans (Atake et al., 2019; Coates et al., 2018; Jayasankar et al., 2020; Maisey et al., 2021; Ørvig, 1951). Among extant chondrichthyans, trabecular mineralization always forms near the surface of cartilage, but the exact mineralization pattern varies. Little skate, along with all other batoids and some selachians examined, have arrayed patterns of discrete trabecular units, similar to the repeating polygonal units of traditional tesserae, supporting their description as trabecular tesserae. On the other hand, a non-arrayed trabecular mineralization pattern, not emphasized in chondrichthyans before, appears to be present in ratfish, catshark, and some other selachians (Berio et al., 2021). To distinguish this pattern from the regular, arrayed patterns of polygonal and trabecular tesserae, we propose the term "non-tesseral trabecular mineralization". Given that some fossil chondrichthyans, such as *Gladbachus*, *Climatius*, and *Doliodus* also appear to display this mineralization pattern in their endoskeletons (Coates et al., 2018; Maisey et al., 2021; Ørvig, 1951), non-tesseral trabecular mineralization might be a new plesiomorphic (ancestral) character of chondrichthyans (Maisey et al., 2021).

Bone-like tissues do not appear to be shared among extant chondrichthyans, while areolar mineralization does seem to be shared (Fig. 7). Morphological and histological features of bone-like tissues in neural arches or tesseral cap zones are present in catshark, little skate, and many other elasmobranch species, but absent in ratfish and *C. monstrosa* (Atake et al.,

373 2019; Berio et al., 2021; Eames et al., 2007; Kemp and Westrin, 1979; Seidel et al., 2020; Seidel
374 et al., 2017; Seidel et al., 2016; Wurmbach, 1932). While these data refute the hypothesis that
375 bone-like tissues generally are a symplesiomorphic (shared ancestral) feature of extant
376 chondrichthyans, they further support the hypothesis that neural arch perichondral bone-like
377 tissue is a synapomorphic (shared derived) character of elasmobranchs, but subsequently lost
378 in several lineages (Atake et al., 2019; Berio et al., 2021; Maisey et al., 2021). On the other
379 hand, similar features of centra are observed in ratfish, catshark, little skate, and many other
380 extant chondrichthyans examined (Atake et al., 2019; Criswell et al., 2017; Dean and Summers,
381 2006; Debiais-Thibaud, 2019; Eames et al., 2007; Porter et al., 2006). Since most data on areolar
382 mineralization focussed on elasmobranchs (Criswell et al., 2017; Eames et al., 2007; Ridewood
383 and MacBride, 1921), histological features of multiple-ringed centra in other chimaera should
384 be determined (Didier, 1995). Stem chondrichthyans did not appear to mineralize their centra,
385 so data from extant chondrichthyans argue that areolar mineralized tissue is likely a
386 synapomorphic character of crown chondrichthyans (Frey et al., 2019; Maisey et al., 2021;
387 Miles, 1970).

388 Cap and body zones are histological terms that traditionally describe chondrichthyan
389 tesserae (Dean and Summers, 2006; Kemp and Westrin, 1979), but data from adult samples of
390 ratfish, catshark, little skate, and several other species argue that the body zone is the only
391 histological zone of endoskeletal mineralization shared by extant chondrichthyans (Fig. 7).
392 Recent histological data of tesserae are few and limited to sharks, skates, and rays, where cap
393 and body zones have been reported (Atake et al., 2019; Berio et al., 2021; Eames et al., 2007;
394 Enault et al., 2015; Kemp and Westrin, 1979; Seidel et al., 2017). While birefringent fibers

395 marked the cap zones in both polygonal and trabecular tesserae in little skate, non-tesseral
396 trabeculae in catshark and ratfish did not have discernible cap zones. In contrast to commonly-
397 accepted knowledge, these catshark data suggest that even sharks do not always have the cap
398 zone. Taken alongside recent published data (Maisey et al., 2021; Pears et al., 2020; Seidel et
399 al., 2020), no living species of chimaera likely has cap zones. On the other hand, Safranin O
400 staining and Col2 immunofluorescence showed that histological body zones generated the
401 mineralized endoskeletal cartilage of ratfish, catshark, and little skate. In total, these data
402 suggest that the ancestral stem chondrichthyan generated most of its endoskeletal
403 mineralization with histological body zones, although as the next paragraph highlights, cap
404 zones might have been lost secondarily in chimaera and some shark species.

405 Digitally segmented 3D regions of micro-CT renderings showed, for the first time, exact
406 spatial correlations between histological zones and mineralization patterns, potentially
407 impacting histological interpretations of fossils. Strikingly, large and laterally extensive cap
408 zones were the basis of the traditional polygonal tesseral mineralization pattern in little skate.
409 Accordingly, similar polygonal tesserae recently described in fossil holocephalans likely have
410 cap zones in addition to body zones and a trabecular tesseral mineralization underlying the
411 polygonal mineralization pattern, and these might have been lost secondarily during
412 holocephalan evolution (Fig. 7; Atake et al., 2019; Pears et al., 2020). Increased descriptive
413 power from synchrotron imaging of polygonal tesserae in fossil elasmobranchs and
414 holocephalans can clarify this point. Two other correlations were identified here in body zones.
415 First, spokes were located in body zones. Second, spoke and non-spoke regions of the body
416 zone comprised the trabecular mineralization patterns, regardless of whether these were

organized as arrayed tesserae or not. Spokes appeared much more spatially organized in polygonal tesserae and trabecular tesserae than in the non-tesseral trabecular mineralization pattern. By extension of the body zone correlation with trabecular mineralization, trabecular mineralization of some fossil elasmobranchs and holocephalans like *Palaeobates polaris* and *Cladoselache* might derive solely from body zones (Maisey et al., 2021; Ørvig, 1951). Given such dramatic variation in extant and fossil chondrichthyans, cellular and molecular mechanisms underlying the evolution of tesseral and non-tesseral mineralization patterns is a wide open field of future study.

Finally, three independent features suggested that the adult ratfish endoskeleton retained embryonic features, compared to elasmobranchs, a phenomenon termed paedomorphism (Garstang, 1922; Liem, 2001). First, tissue mineral density (TMD) was significantly lower in a number of adult ratfish endoskeletal elements, compared to adult catshark and little skate. Reduced TMD might reflect paedomorphism, because as mineralized skeletal tissues develop, their TMD tends to increase (Forbes, 1976). Following up on potential paedomorphism during ratfish centrum development, the TMD of adult ratfish centra was comparable to the TMD of embryonic little skate centra. Second, the morphology of adult ratfish mineralized centra was comparable to the morphology of embryonic little skate mineralized centra. Mineralized centra in chimaeras were thought to be unconstricted (Didier, 1995; Gadow and Abbott, 1895), but micro-CT renderings of ratfish centra showed slight constriction, which was like those of centra in little skate embryos. Third, even histological similarities of centra in little skate embryos and adult ratfish were discovered; both had elongate cell lacunae organized in concentric lamellae only in the mineralized middle layer of

439 the centrum. These findings independently supported a previous assertion that the perichordal
440 sheath in adult chimaeras remained at a stage corresponding to that of embryonic
441 elasmobranchs (Gadow and Abbott, 1895). Given lower TMD in many endoskeletal elements,
442 the chimaera might generally have paedomorphic endoskeletal development. The genetic basis
443 for reduced skeletal mineralization in chimaeras should be investigated further, especially since
444 the only published full chondrichthyan genome was from *Callorhinchus milii* (Callorhinchidae)
445 (Venkatesh et al., 2014), and Callorhinchidae is the only chimaera family, for example, that does
446 not mineralize their centra (Fig. 7; Didier, 1995; Gadow and Abbott, 1895).

447 In summary, analyses of extant and fossil data suggest different features of the
448 chondrichthyan endoskeleton appeared (and disappeared) at different times during evolution
449 of this fascinating clade (Fig. 7). The widespread distribution of non-tesseral trabecular
450 mineralization among fossil stem and extant crown chondrichthyans argue that this is a
451 symplesiomorphic chondrichthyan character. Areolar mineralization is widespread among
452 extant chondrichthyan species, but absent in early stem chondrichthyans, suggesting it evolved
453 in a later stem chondrichthyan that gave rise to holocephalans and elasmobranchs. The
454 presence of tesserae in extant elasmobranchs and the fossil holocephalan *Cobelodus* argues
455 that this trait was lost secondarily in extant holocephalans. Bone-like tissues in cap zones or
456 neural arches appears restricted to extant elasmobranchs. Extant species have correlations
457 between the histological body zone and any form of trabecular mineralization on the one hand,
458 and the cap zone and polygonal tesserae on the other. Given these correlations, the body zone
459 might also be symplesiomorphic for all chondrichthyans, while the cap zone might be
460 synapomorphic for crown chondrichthyans, secondarily lost in extant holocephalans.

Materials and Methods

Specimens

All samples were approved for use under the University of Saskatchewan ethical protocol (AUP 20130092). Vertebrae (precaudal and caudal) from three samples of adult small-spotted catshark with total lengths of 31 cm were provided by the University of Montpellier Aquarium (Planet Ocean Montpellier). Adult, juvenile, and embryonic samples of the little skate were obtained from Marine Biological Labs (Falmouth, MA, USA). Four samples of adult little skate with total lengths (TL) ranging from 43.5 cm – 47.5 cm were sampled (SupTable 1). Little skate juveniles (n=7) were staged by measuring their TL and disc widths (DW) and ranged from 5.5 cm DW, 10 cm TL to 6.5 cm DW, 11 cm TL (SupTable 1; Stehmann, 2002). The average DW and TL of stage 32 embryos (n=6) and stage 33 embryos (n=6) were 3.2 cm DW, 7.5 cm TL and 3.5 cm DW, 8 cm TL, respectively (SupTable 1; Maxwell et al., 2008; Vazquez et al., 2020). Five samples of adult spotted ratfish with total lengths ranging from 28.5 cm to 45 cm were captured by deep-water trawl in the San Juan Islands, WA, frozen within one or two hours of catch, and kept frozen for several years until thawed for experiments (SupTable 1).

Regions of interest, such as ceratohyal, synarcual, and precaudal and caudal vertebrae, were dissected from the little skate, catshark, and ratfish samples (SupTable 1). Dissected tissues were preserved by fixation in 4% paraformaldehyde in PBS (pH 7.4) and dehydrated through a graded ethanol series.

Micro-CT imaging and data processing

483 Desktop micro-CT imaging of ratfish ROIs, little skate ROIs, and catshark precaudal
484 vertebrae was done using SkyScan 1172 desktop microtomograph (Bruker SkyScan, Kontich,
485 Belgium). Desktop micro-CT projections were acquired using a 0.5 mm aluminium filter at 40 kV
486 and 250 µA, 100 ms exposure time, and 10 µm voxel resolution, and reconstructed using
487 NRecon (Bruker SkyScan, Kontich, Belgium). A lower resolution projection (i.e., 26 µm voxel,
488 700 ms exposure time) of an anterior region of the ratfish was acquired in parts (Fig. 1A). Scans
489 from the different parts were later stitched together using Dragonfly v2021.1 (Object Research
490 Systems, Canada). Desktop imaging of catshark caudal vertebrae was performed using CT
491 scanner: EasyTom 150 scanner at 70 kV, 80 µA, 1.43 s exposure time, and 6 µm voxel
492 resolution. Reconstructions were done with Xact software (v11025) images were rendered with
493 Avizo Lite software (v2019.3). Tissue mineral density (TMD) of ratfish, little skate, and catshark
494 ROIs was quantitated on SkyScan 1172 desktop micro-CT images using CTAnalyzer v1.16 (CTAn,
495 Bruker SkyScan, Kontich, Belgium) as previously described (Atake et al., 2019).
496 Synchrotron radiation (SR)-based micro-CT imaging of ratfish and little skate was done
497 on the Biomedical Imaging and Therapy-Insertion Device 05ID-2 (BMIT-ID) line at the Canadian
498 Light Source. SR micro-CT projections were acquired with a 28 keV photon energy, 1.44 µm
499 voxel resolution, 1s exposure time, and a sample to detector distance of 9 cm. Reconstruction
500 of SR micro-CT projections and phase retrieval was done using UFO-KIT software
501 (https://github.com/ufo-kit/ufo-core.git). A delta/beta ratio of 200 was applied during phase
502 retrieval. 3D rendered volumes and 2D virtual slices of reconstructed data were generated with
503 Amira 6.0 (FEI Group, USA). 3D segmentation and color-coding of morphological features were
504 done using segmentation editor tools in Amira.

505

506 **Histological and immunofluorescence assays**

507 Tissues for section histology were not demineralized before sectioning. Tissues were
508 embedded in optimum cutting temperature compound (Tissue Tek, Torrance, CA, United
509 States), and serial tissue sections of 10 µm thickness were made with a Cryostar NX50 cryostat
510 (Fisher Scientific, United States).

511 Tissue sections were stained as described with Safranin O (Ferguson et al., 1998),
512 picrosirius red (Junqueira et al., 1978), or Milligan's Trichrome (Ashique et al., 2022). Alcian
513 blue/Alizarin red staining was done using a modified acid-free protocol (Eames et al., 2011).
514 Briefly, tissues sections were washed with 100 mM Tris pH 7.5/10 mM $MgCl_2$, stained with
515 0.04% Alcian blue/70%EtOH/10mM $MgCl_2$ pH 7.5, taken through graded EtOH series (80%
516 EtOH/100 mM Tris pH 7.5/10 mM MgCl2; 50% EtOH/100 mM Tris pH 7.5; 25% EtOH/100 mM
517 Tris pH 7.5), stained with 0.1% Alizarin red/0.1 % KOH pH 7.5, de-stained with two washes of
518 0.1% KOH, and dehydrated through 25% EtOH, 50% EtOH, 80% EtOH, and 100% EtOH series
519 before coverslipping. Tissue sections were demineralized using 5% EDTA for 10 mins before
520 staining with Safranin O to improve staining of mineralized cartilage.

521 To minimize the chances of tissues falling off slides, tissue sections for
522 immunofluorescence were incubated at 55°C for 15 mins before treatments and then washed
523 with PBST (1xPBS/0.5x triton-X) between subsequent treatments. Tissues were treated
524 separately with trypsin (0.1% in 5%EDTA/1xPBS) and hyaluronidase (0.5% in 1xPBS/0.5x triton-
525 X) at 37°C for 15 mins each. The tissues were blocked with 4% goat serum/2% sheep/1xPBS for
526 1 hr, and then incubated overnight at 4°C with either Col2 antibody (1:100, II-II6B3, Hybridoma

527 Bank) or blocking solution (negative control). Secondary antibody labelling was done using 488-
528 conjugated goat anti-mouse antibody (1:1000, A32723 ThermoFisher Scientific) for 3 hours.
529
530 **Quantitative and statistical analyses**
531 Statistical analyses of TMDs were performed using SPSS V.22 (SPSS). Shapiro–Wilk test was
532 used to test for normal distribution of data. To assess differences among means, one-way
533 analysis of variance (ANOVA) was used followed by Tukey HSD or Games-Howell post hoc
534 analyses, depending upon whether homogeneity of variance assumption (Levene's test) was
535 met or not, respectively.
536

537 ## Data availability

538 Raw data from microCT projections and quantitative measurements have been deposited at
539 Dryad (DOI: 10.5061/dryad.crjdfn3b9) and can be accessed at
540 https://datadryad.org/stash/share/gnKH8kfRoKdHRE9rFGDausGzBZ1VTuCK3DB5gRPkrnp
541

542 ## Acknowledgements

543 This work was funded by Natural Sciences and Engineering Research Council (NSERC) grants
544 RGPIN 435655-201 and RGPIN 2014-05563 awarded to BFE. The authors are very thankful to
545 Adam Summers of Friday Harbor in the San Juan Islands for providing the spotted ratfish
546 samples and some feedback on the spotted ratfish data. Research described in this paper was
547 performed at the BMIT facility at the Canadian Light Source, which is supported by Canada
548 Foundation for Innovation, Natural Sciences and Engineering Research Council of Canada, the

University of Saskatchewan, Western Economic Diversification Canada, the National Research Council Canada, and the Canadian Institutes of Health Research. We acknowledge the MRI platform member of the national infrastructure France-BioImaging supported by the French National Research Agency (ANR-10-INBS- 04, “Investments for the future”), the labex CEMEB (ANR-10-LABX-0004) and NUMEV (ANR-10-LABX-0020).

555 **Figure legends**

556 **Figure 1. Mineralized tissues were abundant in the spotted ratfish, but they had lower tissue**
557 **mineral density (TMD) compared to the little skate and the small-spotted catshark.** (**A**)
558 Photograph of the ratfish *Hydrolagus colliei* illustrating the anterior region that was micro-CT
559 imaged. (**B-G**) Micro-CT 3D renderings of the anterior region of ratfish (B) showed mineralized
560 tissues in neural arches, basidorsals, and centra in segmented vertebrae (C,D), in the ceratohyal
561 and other skeletal elements in the pharyngeal skeleton (E), and in the fused vertebral synarcual
562 (F,G). (**H**) Comparative quantitative analyses showed that TMD of the synarcual, neural arch,
563 and centra in ratfish were significantly lower than TMDs of same regions in little skate and
564 catshark. Abbreviations: A, anterior; bb, basibranchial; bd, basidorsal; bh, basihyal; c, centrum
565 cb, ceratobranchial; ch, ceratohyal; D, dorsal; hbs, hypobranchials; L, left; MK, Meckel's; na,
566 neural arch; P, posterior; R, right; snf, spinal nerve foramina; V, ventral. * indicates statistically
567 significant comparison ($p<0.05$). Scale bars: as indicated.

568

569 **Figure 2. Ratfish lack neural arch bone-like tissue.** (**A-C**) Micro-CT 3D renderings showed a
570 non-continuous pattern of mineralized tissues in neural arches of segmented vertebrae in
571 ratfish (A), compared to the continuous mineralization pattern of compact, bone-like tissue in
572 catshark (B) and little skate (C). (**D-F**) Micro-CT 2D virtual slices showed that mineralized tissues
573 (arrows) in ratfish neural arches were restricted to medial and lateral peripheries (D), whereas
574 the bone-like tissue in catshark and little skate extended much deeper in the neural arch (E,F).
575 (**G-I**) Alizarin red staining of histological sections confirmed micro-CT representation of
576 mineralization patterns in ratfish (G), catshark (H), and little skate (I) neural arches, and Alcian

577 blue revealed cartilaginous regions. (**J-L**) Picrosirius red staining did not reveal birefringent
578 collagen fibers in ratfish neural arches (J), but such staining was abundant in bone-like tissues in
579 catshark (K) and little skate (L). Birefringent fibers (likely reticular) were present in muscles
580 (vertical arrows) on the lateral sides of neural arches in all species. Col2 immunostaining
581 confirmed Alcian blue staining, identifying cartilage regions in all species. The neural arch core
582 in catshark (K) and little skate (L) consisted of mostly unmineralized cartilage and mineralized
583 cartilage, respectively. Abbreviations: 2D, two-dimensional; 3D, three-dimensional; Ab, Alcian
584 blue; Ar, Alizarin red; BLT, bone-like tissue; c, cartilage; Col2, collagen type 2; D, dorsal; IF,
585 immunofluorescence; L, lateral; M, medial; MC, mineralized cartilage; PSR, picrosirius red; V,
586 ventral. Scale bars: as indicated.
587
588 **Figure 3. Ratfish, catshark, and little skate all showed trabecular mineralization, but ratfish**
589 **and catshark did not have a bone-like cap zone.** (**A-H**) Micro-CT renderings of the ratfish
590 ceratohyal (A,E) and catshark caudal vertebra (B,F) demonstrated non-tesseral trabecular
591 mineralization, while little skate hyomandibula had tesseral trabecular mineralization (C,G).
592 Little skate precaudal vertebra had tesseral polygonal mineralization (D,H) overlying tesseral
593 trabecular mineralization (H'). Regions for hi-mag views in panels E-H' are indicated in
594 corresponding panels of A-D. (**I-P**) Alcian blue/Alizarin red and Safranin O/fast green staining of
595 histological sections demonstrated that the body zone of non-tesseral or tesseral trabecular
596 mineralized tissues in ratfish (I,M), catshark (J,N), and little skate (K,L,O,P) was mineralized
597 cartilage, while the cap zone of tesseral polygonal mineralization was bone-like (K,L,O,P). (**Q-T**)
598 Col2 immunostaining of adjacent sections to panels I-P confirmed cartilage regions in all

599 species, while picrosirius red staining confirmed the bone-like tesseral cap zone in little skate.
600 Abbreviations: Ab, Alcian blue; Ar, Alizarin red; Bz, body zone; c, cartilage; Col2, collagen type 2;
601 Cz, cap zone; D, dorsal; IF, immunofluorescence; L, lateral; M, medial; PSR, picrosirius red; NA,
602 neural arch; NS, neural spine; V, ventral. Scale bars: as indicated.
603
604 **Figure 4. Micro-CT segmentation clearly correlated histological features and mineralization**
605 **patterns.** (**A-C**) Trichrome staining showed that spokes in the body zone of ratfish non-tesseral
606 trabeculae (A) or little skate trabecular (B) or polygonal (C) tesserae had low cellularity and
607 were unstained, while intense acid fuchsin staining marked the smaller and larger cap zones of
608 little skate trabecular (B) and polygonal (C) tesserae, respectively. (**D-I**) 3D renderings of
609 synchrotron micro-CT data showed that hypermineralized spokes (*, segmented in blue) were
610 in the body zone of ratfish non-tesseral trabeculae (D,G) or little skate trabecular (E,H) or
611 polygonal (F,I) tesserae. Tesseral cap zones could also be segmented clearly (red) in little skate
612 (E,F,H,I). (**J-O**) Segmented 3D renderings demonstrated that spokes in ratfish were patchy in
613 deep (J) or superficial (M) views, while little skate spokes displayed a radiating pattern
614 traversing most of the trabecular patterns in either trabecular (K,N) or polygonal (L,O) tesserae.
615 The smaller cap zone in trabecular tesserae (N) was not laterally extensive enough to display a
616 superficial polygonal pattern like that of polygonal tesserae (O). Abbreviations: Bz, body zone;
617 Cz, cap zone. Scale bars: as indicated.
618
619 **Figure 5. Ratfish centra had the same features as areolar mineralized tissues in little skate**
620 **and catshark.** (**A-C**) Micro-CT renderings demonstrated that centra in ratfish (A), catshark (B),

621 and little skate (C) all had a compact mineralization, but ratfish centra were organized in
622 multiple rings and did not display the gross biconcave morphology seen in catshark or little
623 skate. (**D-O**) Alcian blue/Alizarin red and Safranin O section histology and Col2 immunostaining
624 demonstrated that mineralized centra in ratfish (D,G,J), catshark (E,H,K), and little skate (F,I,L)
625 all comprised a middle layer with elongate lacunae in concentric lamellae, but in ratfish this was
626 mineralized cartilage, while catshark and little skate had little to no Safranin O or Col2 staining,
627 respectively, in this region. Catshark mineralized centra also comprised the outer layer, while
628 little skate mineralized centra also comprised both inner and outer layers. These additional
629 centra layers had rounded cells embedded in matrix of weak Safranin O staining and Col2
630 immunofluorescence. Regions for hi-mag views in panels G-O are indicated in corresponding
631 panels of D-F; regions for hi-mag inserts in panels G-I are indicated in those panels.
632 Abbreviations: A, anterior; Ab, Alcian blue; Ar, Alizarin red; c, cartilage; Col2, collagen type 2; D,
633 dorsal; IF, immunofluorescence; IL, inner layer; L, lateral; M, medial, OL, outer layer; P,
634 posterior; V, ventral. Scale bars: as indicated; inserts in G-I are 20 µm.
635
636 **Figure 6. Morphological and histological features of centra were shared between little skate**
637 **embryos and juveniles and adult ratfish.** (**A-D**) Desktop micro-CT renderings showed centra
638 and other mineralized structures in vertebral segments (dashed lines) of little skate embryos
639 and juveniles (A-C) and adult ratfish (D). (**E-H**) Synchrotron micro-CT renderings of centra in
640 little skate embryos and juveniles (E-G) and adult ratfish (H) showed that centra in the ratfish
641 were slightly constricted, like those of little skate embryos (red arrows). (**I-K**) Alcian
642 blue/Alizarin red section histology showed that areolar mineralized tissue constituted the only

643 centra layer in little skate embryos (I,J), whereas an outer mineralized centra layer was present
644 in 6.5 cm DW juveniles (K). (**L**) Tissue mineral density (TMD) of centra in ratfish was similar to
645 those of stage 33 embryos and 6.5 cm DW juveniles of little skate. Abbreviation: A, anterior; Ab,
646 Alcian blue; Ar, Alizarin red; bd, basidorsal; C, centrum; HA, haemal arch; L, lateral; M, medial;
647 NA, neural arch; OL, outer layer; P, posterior.* indicates statistically significant comparison
648 (p<0.05). Scale bars: as indicated.
649
650 **Figure 7. Character states of mineralized tissues in various extant and fossil chondrichthyan**
651 **species suggest shared and derived features.** Non-tesseral trabecular mineralization (NTT) is
652 likely a symplesiomorphic (shared ancestral) character of stem and crown chondrichthyans,
653 because it is pervasive in fossil (Coates et al., 2018; Maisey et al., 2021; Pears et al., 2020) and
654 extant (Berio et al., 2021; Seidel et al., 2020) chondrichthyans. Polygonal (PT) and trabecular
655 (TT) tesseral mineralization patterns appear to be absent in extant holocephalans and stem
656 chondrichthyans, but their presence in some extant elasmobranchs (Atake et al., 2019; Berio et
657 al., 2022; Berio et al., 2021; Seidel et al., 2016; Wilga and Ferry, 2015) and a fossil holocephalan
658 (Pears et al., 2020) suggest that these tesseral mineralizations are synapomorphic (shared
659 derived) characters of crown chondrichthyans, subsequently lost in extant holocephalans.
660 Areolar mineralized tissue is present in extant elasmobranchs (Atake et al., 2019; Berio et al.,
661 2021; Criswell et al., 2017; Eames et al., 2007; Porter et al., 2016; Seidel et al., 2020) and
662 holocephalans, but its absence in stem chondrichthyans suggests that it is a synapomorphic
663 character of crown chondrichthyans. The absence of neural arch bone-like tissue (BLT) in
664 holocephalans further supports the conclusion that it is a synapomorphic character of

665 elasmobranchs. The presence of a histological body zone in either tesseral or non-tesseral
666 mineralized tissues of stem and crown chondrichthyans suggests that the body zone is a
667 symplesiomorphic character of all chondrichthyans. The histological cap zone in some
668 elasmobranchs (Atake et al., 2019; Berio et al., 2021; Seidel et al., 2016; Wilga and Ferry, 2015),
669 along with the inference that polygonal tesserae in a fossil holocephalan means that they had
670 cap zones (Pears et al., 2020), suggests that the cap zone is also a synapomorphic character of
671 crown chondrichthyans. 0, 1, and ? indicate negative, positive, and unknown observations,
672 respectively, of characters for the listed species. References to data from the listed species are
673 cited in the legend
674

675 **References**

676 Arratia, G., Schultze, H.P., Casciotta, J., 2001. Vertebral column and associated elements in dipnoans and
677 comparison with other fishes: development and homology. J Morphol 250, 101-172 DOI:
678 10.1002/jmor.1062.

679 Ashique, A.M., Atake, O.J., Ovens, K., Guo, R., Pratt, I.V., Detrich III, H.W., Cooper, D.M., Desvignes, T.,
680 Postlethwait, J.H., Eames, B.F., 2022. Bone microstructure and bone mineral density are not systemically
681 different in Antarctic icefishes and related Antarctic notothenioids. Journal of Anatomy 240, 34-49 DOI:
682 https://doi.org/10.1111/joa.13537.

683 Atake, O.J., Cooper, D.M.L., Eames, B.F., 2019. Bone-like features in skate suggest a novel elasmobranch
684 synapomorphy and deep homology of trabecular mineralization patterns. Acta Biomater 84, 424-436
685 DOI: 10.1016/j.actbio.2018.11.047.

686 Atake, O.J., Eames, B.F., 2021. Mineralized Cartilage and Bone-Like Tissues in Chondrichthyans Offer
687 Potential Insights Into the Evolution and Development of Mineralized Tissues in the Vertebrate
688 Endoskeleton. Frontiers in Genetics 12 DOI: 10.3389/fgene.2021.762042.

Berio, F., Bayle, Y., Riley, C., Larouche, O., Cloutier, R., 2022. Phenotypic regionalization of the vertebral column in the thorny skate Amblyraja radiata: Stability and variation. Journal of Anatomy 240, 253-267 DOI: https://doi.org/10.1111/joa.13551.

Berio, F., Broyon, M., Enault, S., Pirot, N., López-Romero, F.A., Debiais-Thibaud, M., 2021. Diversity and Evolution of Mineralized Skeletal Tissues in Chondrichthyans. Frontiers in Ecology and Evolution 9, 223 DOI: 10.3389/fevo.2021.660767.

Bordat, C., 1987. Étude ultrastructurale de l'os des vertèbres du Sélacien Scyliorhinus canicula L. Canadian Journal of Zoology 65, 1435-1444 DOI: 10.1139/z87-226.

Claeson, K.M., 2011. The synarcual cartilage of batoids with emphasis on the synarcual of Rajidae. J Morphol 272, 1444-1463 DOI: 10.1002/jmor.10996.

Clement, J., 1992. Re-examination of the fine structure of endoskeletal mineralization in chondrichthyans: implications for growth, ageing and calcium homeostasis. Marine and Freshwater Research 43, 157-181.

Coates, M.I., Finarelli, J.A., Sansom, I.J., Andreev, P.S., Criswell, K.E., Tietjen, K., Rivers, M.L., La Riviere, P.J., 2018. An early chondrichthyan and the evolutionary assembly of a shark body plan. Proc Biol Sci 285, 20172418 DOI: 10.1098/rspb.2017.2418.

Criswell, K.E., Coates, M.I., Gillis, J.A., 2017. Embryonic development of the axial column in the little skate, *Leucoraja erinacea*. J Morphol 278, 300-320 DOI: 10.1002/jmor.20637.

Criswell, K.E., Gillis, J.A., 2020. Resegmentation is an ancestral feature of the gnathostome vertebral skeleton. Elife 9, e51696 DOI: 10.7554/eLife.51696.

Daniel, J.F., 1934. The elasmobranch fishes. University of California press, Berkeley, California.

Dean, M.N., Bizzarro, J.J., Clark, B., Underwood, C.J., Johanson, Z., 2017. Large batoid fishes frequently consume stingrays despite skeletal damage. Royal Society Open Science 4, 170674 DOI: doi:10.1098/rsos.170674.

Dean, M.N., Summers, A.P., 2006. Mineralized cartilage in the skeleton of chondrichthyan fishes. Zoology (Jena) 109, 164-168 DOI: 10.1016/j.zool.2006.03.002.

715 Debiais-Thibaud, M., 2018. The Evolution of Endoskeletal Mineralisation in Chondrichthyan Fish,
716 Evolution and development of fishes. Cambridge University Press, pp. 110-125.

717 Debiais-Thibaud, M., 2019. The Evolution of Endoskeletal Mineralisation in Chondrichthyan Fish:
718 Development, Cells and Molecules, in: Underwood, C., Richter, M., Johanson, Z. (Eds.), Evolution and
719 Development of Fishes. Cambridge University Press, Cambridge, pp. 110-125.

720 Didier, D.A., 1995. Phylogenetic systematics of extant chimaeroid fishes (Holocephali, Chimaeroidei).
721 American Museum of Natural History, New York.

722 Eames, B.F., Allen, N., Young, J., Kaplan, A., Helms, J.A., Schneider, R.A., 2007. Skeletogenesis in the swell
723 shark *Cephaloscyllium ventriosum*. J Anat 210, 542-554 DOI: 10.1111/j.1469-7580.2007.00723.x.

724 Eames, B.F., Yan, Y.-L., Swartz, M.E., Levic, D.S., Knapik, E.W., Postlethwait, J.H., Kimmel, C.B., 2011.
725 Mutations in fam20b and xylt1 reveal that cartilage matrix controls timing of endochondral ossification
726 by inhibiting chondrocyte maturation. PLoS Genetics 7, e1002246 DOI: 10.1371/journal.pgen.1002246.

727 Enault, S., Munoz, D.N., Silva, W.T., Borday-Birraux, V., Bonade, M., Oulion, S., Venteo, S., Marcellini, S.,
728 Debiais-Thibaud, M., 2015. Molecular footprinting of skeletal tissues in the catshark *Scyliorhinus*
729 *canicula* and the clawed frog *Xenopus tropicalis* identifies conserved and derived features of vertebrate
730 calcification. Front Genet 6, 283 DOI: 10.3389/fgene.2015.00283.

731 Ferguson, C.M., Miclau, T., Hu, D., Alpern, E., Helms, J.A., 1998. Common molecular pathways in skeletal
732 morphogenesis and repair. Ann N Y Acad Sci 857, 33-42 DOI: 10.1111/j.1749-6632.1998.tb10105.x.

733 Forbes, G.B., 1976. Calcium accumulation by the human fetus. Pediatrics 57, 976-977 DOI:
734 10.1542/peds.57.6.976.

735 Frey, L., Coates, M., Ginter, M., Hairapetian, V., Rucklin, M., Jerjen, I., Klug, C., 2019. The early
736 elasmobranch *Phoebodus*: phylogenetic relationships, ecomorphology and a new time-scale for shark
737 evolution. Proc Biol Sci 286, 20191336 DOI: 10.1098/rspb.2019.1336.

738 Gadow, H.F., Abbott, E., 1895. IV. On the evolution of the vertebral column of fishes. Philosophical
739 Transactions of the Royal Society of London. (B.) 186, 163-221 DOI: 10.1098/rstb.1895.0004.

740 Garstang, W., 1922. The Theory of Recapitulation: A Critical Re-statement of the Biogenetic Law.
741 Zoological Journal of the Linnean Society 35, 81-101 DOI: 10.1111/j.1096-3642.1922.tb00464.x.

742 Gillis, J.A., Rawlinson, K.A., Bell, J., Lyon, W.S., Baker, C.V., Shubin, N.H., 2011. Holocephalan embryos
743 provide evidence for gill arch appendage reduction and opercular evolution in cartilaginous fishes. Proc
744 Natl Acad Sci U S A 108, 1507-1512 DOI: 10.1073/pnas.1012968108.

745 Goldring, M.B., Tsuchimochi, K., Ijiri, K., 2006. The control of chondrogenesis. J Cell Biochem 97, 33-44
746 DOI: 10.1002/jcb.20652.

747 Golub, E.E., 2009. Role of matrix vesicles in biomineralization. Biochim Biophys Acta 1790, 1592-1598
748 DOI: 10.1016/j.bbagen.2009.09.006.

749 Herbert, A.M., Dean, M.N., Summers, A.P., Wilga, C.D., 2022. Biomechanics of the jaws of spotted
750 ratfish. Journal of Experimental Biology 225 DOI: 10.1242/jeb.243748.

751 Janvier, P., 1996. Early vertebrates. Oxford University Press.

752 Jayasankar, A.K., Seidel, R., Hosny, A., Weaver, J.C., Fratzl, P., Chen, J., Dean, M.N., 2020. Multi-scale
753 modeling and mechanical performance characterization of stingray skeleton-inspired tessellations.
754 Journal of the Mechanics and Physics of Solids 138, 103906 DOI: 10.1016/j.jmps.2020.103906.

755 Johanson, Z., Boisvert, C., Maksimenko, A., Currie, P., Trinajstic, K., 2015. Development of the Synarcual
756 in the Elephant Sharks (Holocephali; Chondrichthyes): Implications for Vertebral Formation and Fusion.
757 PLoS One 10, e0135138 DOI: 10.1371/journal.pone.0135138.

758 Johanson, Z., Trinajstic, K., Carr, R., Ritchie, A., 2012. Evolution and development of the synarcual in
759 early vertebrates. Zoomorphology 132, 95-110 DOI: 10.1007/s00435-012-0169-9.

760 Junqueira, L.C., Cossermelli, W., Brentani, R., 1978. Differential staining of collagens type I, II and III by
761 Sirius Red and polarization microscopy. Arch Histol Jpn 41, 267-274 DOI: 10.1679/aohc1950.41.267.

762 Kemp, N.E., Westrin, S.K., 1979. Ultrastructure of calcified cartilage in the endoskeletal tesserae of
763 sharks. J Morphol 160, 75-109 DOI: 10.1002/jmor.1051600106.

764 Kölliker, A., 1860. Über das Ende der Wirbelsäule der Ganoiden und einiger Teleostier. W. Engelmann.

765 Liem, K.F., Bemis, Willam E, Walker, Warren F, and Grande, Lance, 2001. Functional anatomy of the
766 vertebrates: an evolutionary perspective, Third ed. Brooks/Cole, Belmont, CA.

767 Lowenstam, H.A., 1981. Minerals formed by organisms. Science 211, 1126-1131 DOI:
768 10.1126/science.7008198.

769 Maisey, J.G., 2013. The diversity of tessellated calcification in modern and extinct chondrichthyans.
770 Revue de Paléobiologie 32, 355-371.

771 Maisey, J.G., Denton, J.S.S., Burrow, C., Pradel, A., 2021. Architectural and ultrastructural features of
772 tessellated calcified cartilage in modern and extinct chondrichthyan fishes. J Fish Biol 98, 919-941 DOI:
773 10.1111/jfb.14376.

774 Marramà, G., Schultz, O., Kriwet, J., 2019. A new Miocene skate from the Central Paratethys (Upper
775 Austria): the first unambiguous skeletal record for the Rajiformes (Chondrichthyes: Batomorphii). J Syst
776 Palaeontol 17, 937-960 DOI: 10.1080/14772019.2018.1486336.

777 Maxwell, E.E., Fröbisch, N.B., Heppleston, A.C., 2008. Variability and Conservation in Late
778 Chondrichthyan Development: Ontogeny of the Winter Skate (Leucoraja ocellata). The Anatomical
779 Record 291, 1079-1087 DOI: https://doi.org/10.1002/ar.20719.

780 Miles, R.S., 1970. Remarks on the Vertebral Column and Caudal Fin of Acanthodian Fishes. Lethaia 3,
781 343-362 DOI: 10.1111/j.1502-3931.1970.tb00828.x.

782 Omelon, S., Georgiou, J., Variola, F., Dean, M.N., 2014. Colocation and role of polyphosphates and
783 alkaline phosphatase in apatite biomineralization of elasmobranch tesserae. Acta Biomater 10, 3899-
784 3910 DOI: 10.1016/j.actbio.2014.06.008.

785 Ørvig, T., 1951. The endoskeleton, with remarks on the hard tissues of lower vertebrates in general,
786 Histologic studies of Placoderms and fossil Elasmobranchs. Almqvist & Wiksell, Stockholm, pp. 321-454.

787 Pears, J.B., Johanson, Z., Trinajstic, K., Dean, M.N., Boisvert, C.A., 2020. Mineralization of the
788 *Callorhinchus* Vertebral Column (Holocephali; Chondrichthyes). Front Genet 11, 571694 DOI:
789 10.3389/fgene.2020.571694.

790 Peignoux-Deville, J., Lallier, F., Vidal, B., 1982. Evidence for the presence of osseous tissue in dogfish
791 vertebrae. Cell Tissue Res 222, 605-614 DOI: 10.1007/BF00213858.

792 Porter, M.E., Beltrán, J.L., Koob, T.J., Summers, A.P., 2006. Material properties and biochemical
793 composition of mineralized vertebral cartilage in seven elasmobranch species (Chondrichthyes). J Exp
794 Biol 209, 2920-2928 DOI: 10.1242/jeb.02325.

795 Porter, M.E., Ewoldt, R.H., Long, J.H., Jr, 2016. Automatic control: the vertebral column of dogfish sharks
796 behaves as a continuously variable transmission with smoothly shifting functions. Journal of
797 Experimental Biology 219, 2908-2919 DOI: 10.1242/jeb.135251.

798 Ridewood, W., MacBride, E.W., 1921. VIII.—On the calcification of the vertebral centra in sharks and
799 rays. Philosophical Transactions of the Royal Society of London. Series B, Containing Papers of a
800 Biological Character 210, 311-407 DOI: 10.1098/rstb.1921.0008.

801 Rossert, J., de Crombrugghe, B., 2002. Type I collagen: structure, synthesis, and regulation, Principles of
802 bone biology. Elsevier, pp. 189-XVIII.

803 Seidel, R., Blumer, M., Chaumel, J., Amini, S., Dean, M.N., 2020. Endoskeletal mineralization in chimaera
804 and a comparative guide to tessellated cartilage in chondrichthyan fishes (sharks, rays and chimaera). J R
805 Soc Interface 17, 20200474 DOI: 10.1098/rsif.2020.0474.

806 Seidel, R., Blumer, M., Pechriggl, E.J., Lyons, K., Hall, B.K., Fratzl, P., Weaver, J.C., Dean, M.N., 2017.
807 Calcified cartilage or bone? Collagens in the tessellated endoskeletons of cartilaginous fish (sharks and
808 rays). J Struct Biol 200, 54-71 DOI: 10.1016/j.jsb.2017.09.005.

809 Seidel, R., Lyons, K., Blumer, M., Zaslansky, P., Fratzl, P., Weaver, J.C., Dean, M.N., 2016. Ultrastructural
810 and developmental features of the tessellated endoskeleton of elasmobranchs (sharks and rays). J Anat
811 229, 681-702 DOI: 10.1111/joa.12508.

812 Smith, M., Manzanares, E., Underwood, C., Healy, C., Clark, B., Johanson, Z., 2020. Holocephalan
813 (Chondrichthyes) dental plates with hypermineralized dentine as a substitute for missing teeth through
814 developmental plasticity. J Fish Biol 97, 16-27 DOI: 10.1111/jfb.14302.

815 Smith, M.M., Hall, B.K., 1990. Development and evolutionary origins of vertebrate skeletogenic and
816 odontogenic tissues. Biol Rev Camb Philos Soc 65, 277-373 DOI: 10.1111/j.1469-185x.1990.tb01427.x.

Stehmann, M.F., 2002. Proposal of a maturity stages scale for oviparous and viviparous cartilaginous fishes (Pisces, Chondrichthyes). Archive of Fishery and Marine research 50, 23-48.

Vazquez, D.M., Díaz de Astarloa, J.M., Gabbanelli, V., Mabragaña, E., 2020. Comparative embryonic development patterns in three deep-water skates from the southwest Atlantic. Deep Sea Research Part I: Oceanographic Research Papers 161, 103301 DOI: 10.1016/j.dsr.2020.103301.

Venkatesh, B., Lee, A.P., Ravi, V., Maurya, A.K., Lian, M.M., Swann, J.B., Ohta, Y., Flajnik, M.F., Sutoh, Y., Kasahara, M., Hoon, S., Gangu, V., Roy, S.W., Irimia, M., Korzh, V., Kondrychyn, I., Lim, Z.W., Tay, B.-H., Tohari, S., Kong, K.W., Ho, S., Lorente-Galdos, B., Quilez, J., Marques-Bonet, T., Raney, B.J., Ingham, P.W., Tay, A., Hillier, L.W., Minx, P., Boehm, T., Wilson, R.K., Brenner, S., Warren, W.C., 2014. Elephant shark genome provides unique insights into gnathostome evolution. Nature 505, 174-179 DOI: 10.1038/nature12826.

Wilga, C.A.D., Ferry, L.A., 2015. 4 - Functional Anatomy and Biomechanics of Feeding in Elasmobranchs, in: Shadwick, R.E., Farrell, A.P., Brauner, C.J. (Eds.), Fish Physiology. Academic Press, pp. 153-187.

Wurmbach, H., 1932. Das Wachstum des Selachierwirbels und seiner Gewebe. Zool Jahrb (Abt Anat Ont Tiere) 55, 1-136.

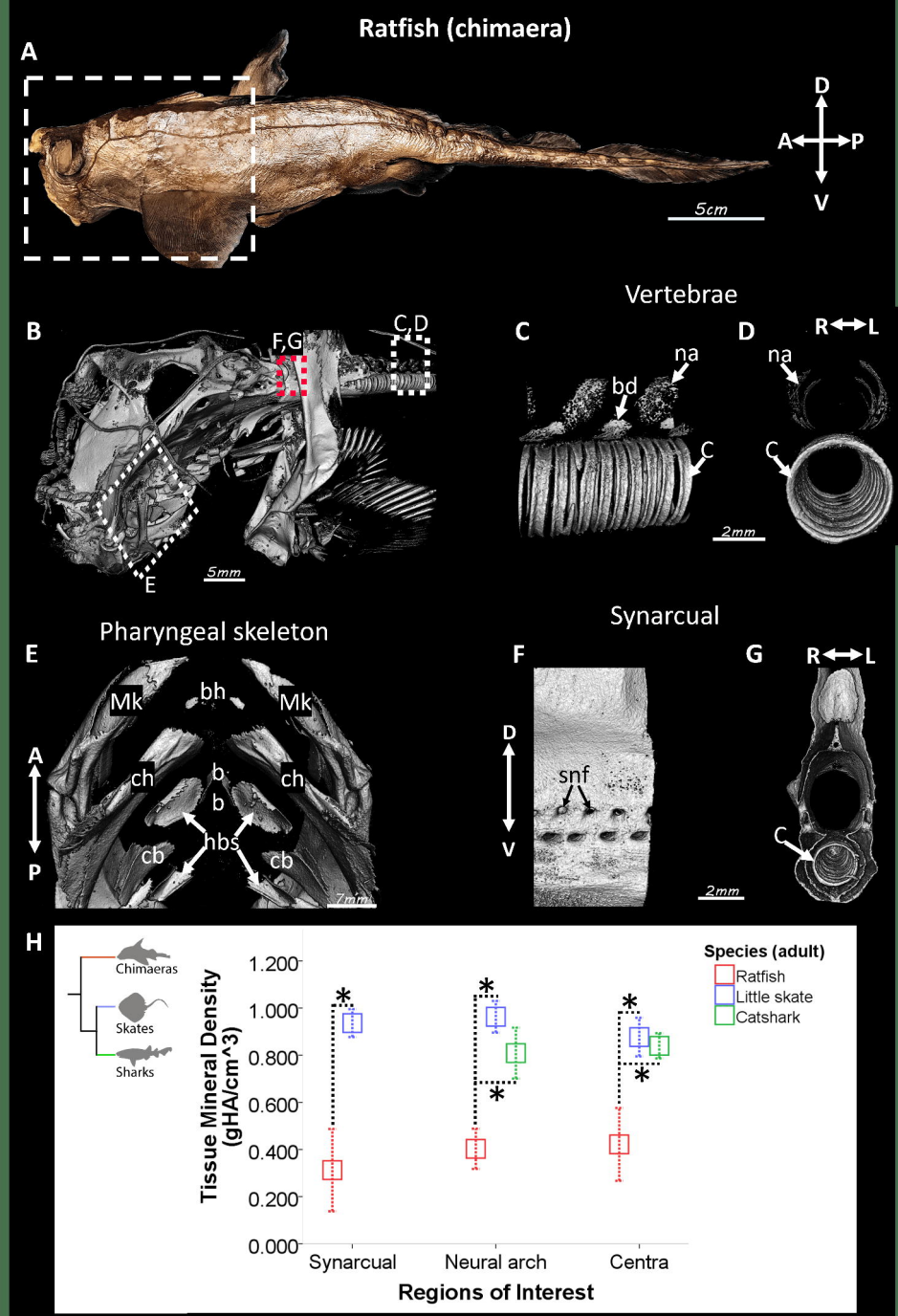
Ratfish (chimaera)
A
D
A
P
V
5cm
B
F,G
C,D
E
5mm
Vertebrae
C
na
bd
C
2mm
D
R
L
na
C
Pharyngeal skeleton
E
Mk
bh
Mk
A
P
ch
b
b
ch
hbs
cb
cb
7mm
Synarcual
F
D
V
snf
2mm
G
R
L
C
H
Chimaeras
Skates
Sharks
Tissue Mineral Density (gHA/cm^3)
1.200
1.000
0.800
0.600
0.400
0.200
0.000
Synarcual
Neural arch
Centra
Regions of Interest
Species (adult)
Ratfish
Little skate
Catshark

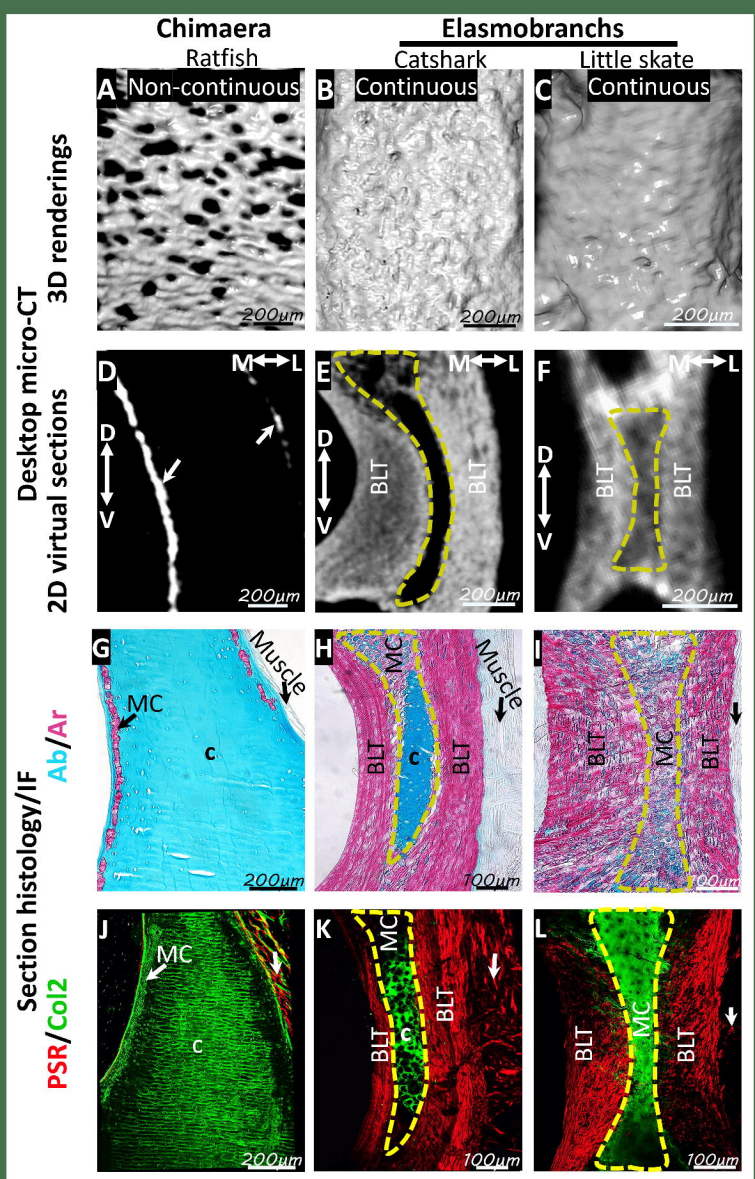

Chimaera
Ratfish
Elasmobranchs
Catshark
Little skate
Desktop micro-CT
3D renderings
2D virtual sections
Section histology/IF
Ab/Ar
PSR/Col2
A Non-continuous
B Continuous
C Continuous
D
E
F
M↔L
D
V
BLT
G
H
I
J
K
L
MC
c
Muscle
200µm
100µm

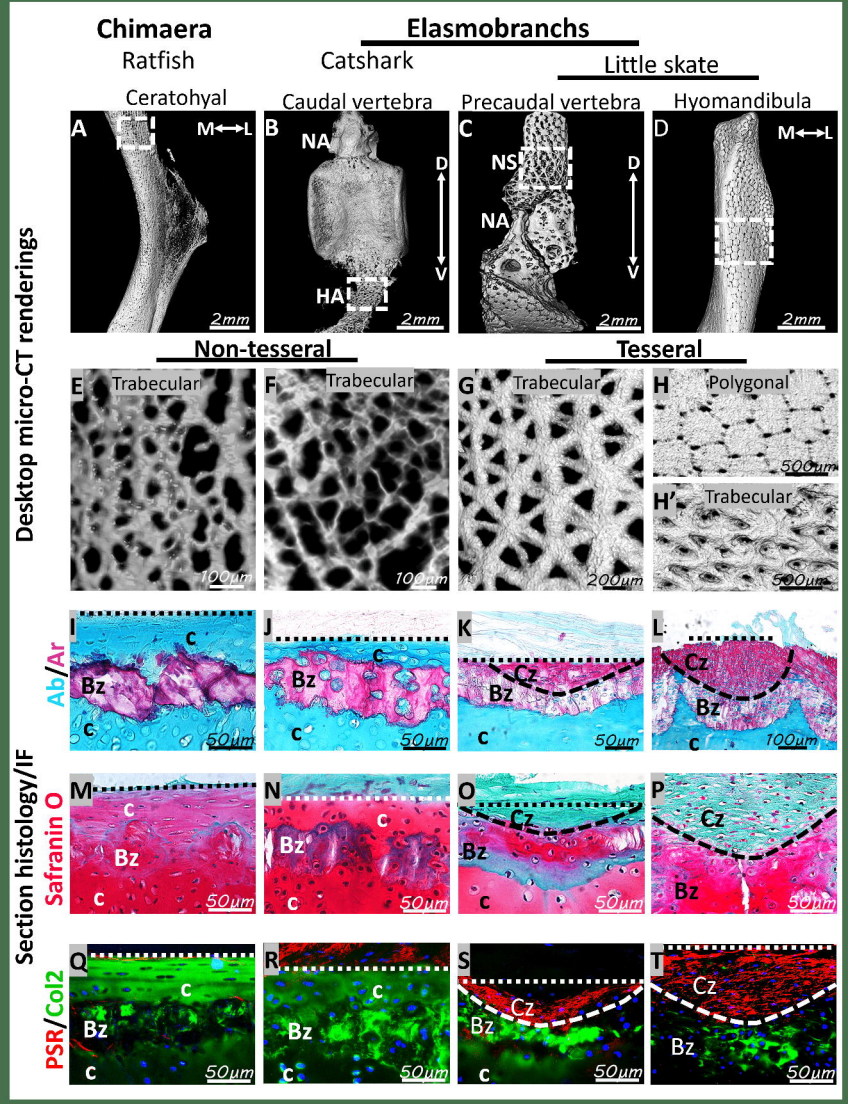
Chimaera
Ratfish
Elasmobranchs
Catshark
Little skate
Ceratohyal
Caudal vertebra
Precaudal vertebra
Hyomandibula
Desktop micro-CT renderings
A
M↔L
2mm
B
NA
HA
D
V
2mm
C
NS
NA
D
V
2mm
D
M↔L
2mm
Non-tesseral
Tesseral
E
Trabecular
100µm
F
Trabecular
100µm
G
Trabecular
200µm
H
Polygonal
500µm
H'
Trabecular
500µm
Section histology/IF
Ab/Ar
I
c
Bz
c
50µm
J
c
Bz
c
50µm
K
Cz
Bz
c
50µm
L
Cz
Bz
c
100µm
Safranin O
M
c
Bz
c
50µm
N
c
Bz
c
50µm
O
Cz
Bz
c
50µm
P
Cz
Bz
50µm
PSR/Col2
Q
c
Bz
c
50µm
R
c
Bz
c
50µm
S
Cz
Bz
c
50µm
T
Cz
Bz
50µm

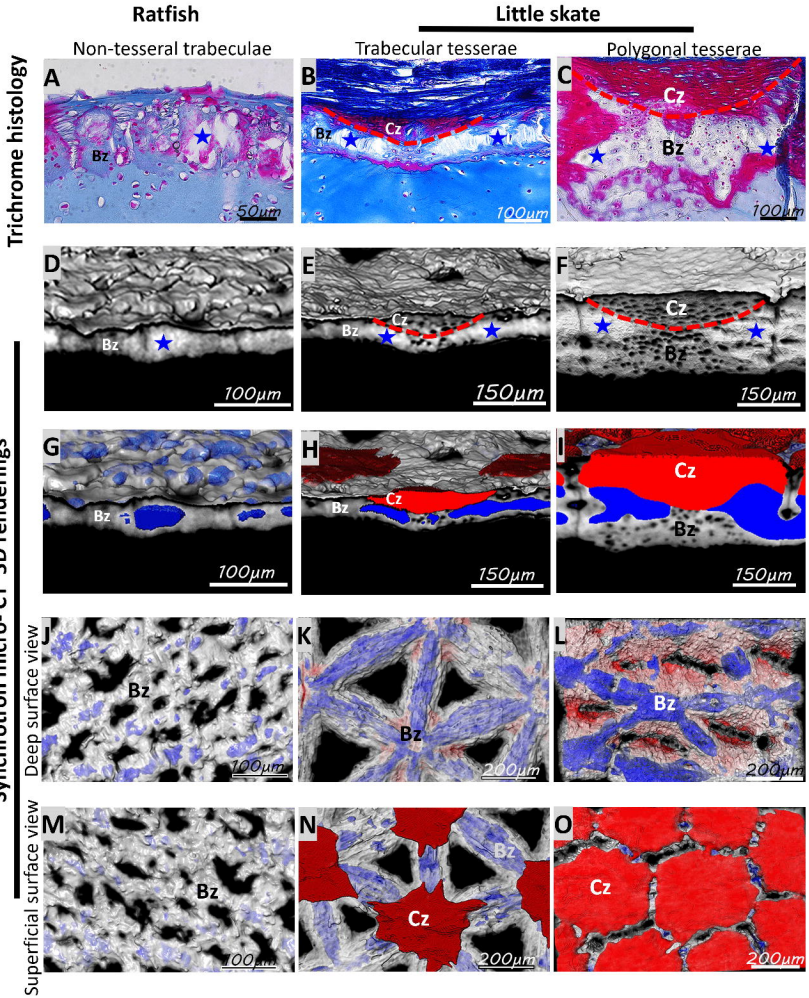
Ratfish
Little skate
Non-tesseral trabeculae
Trabecular tesserae
Polygonal tesserae
Trichrome histology
Synchrotron micro- CT 3D renderings
Deep surface view
Superficial surface view
A
B
C
D
E
F
G
H
I
J
K
L
M
N
O
Bz
Cz
50µm
100µm
150µm
200µm

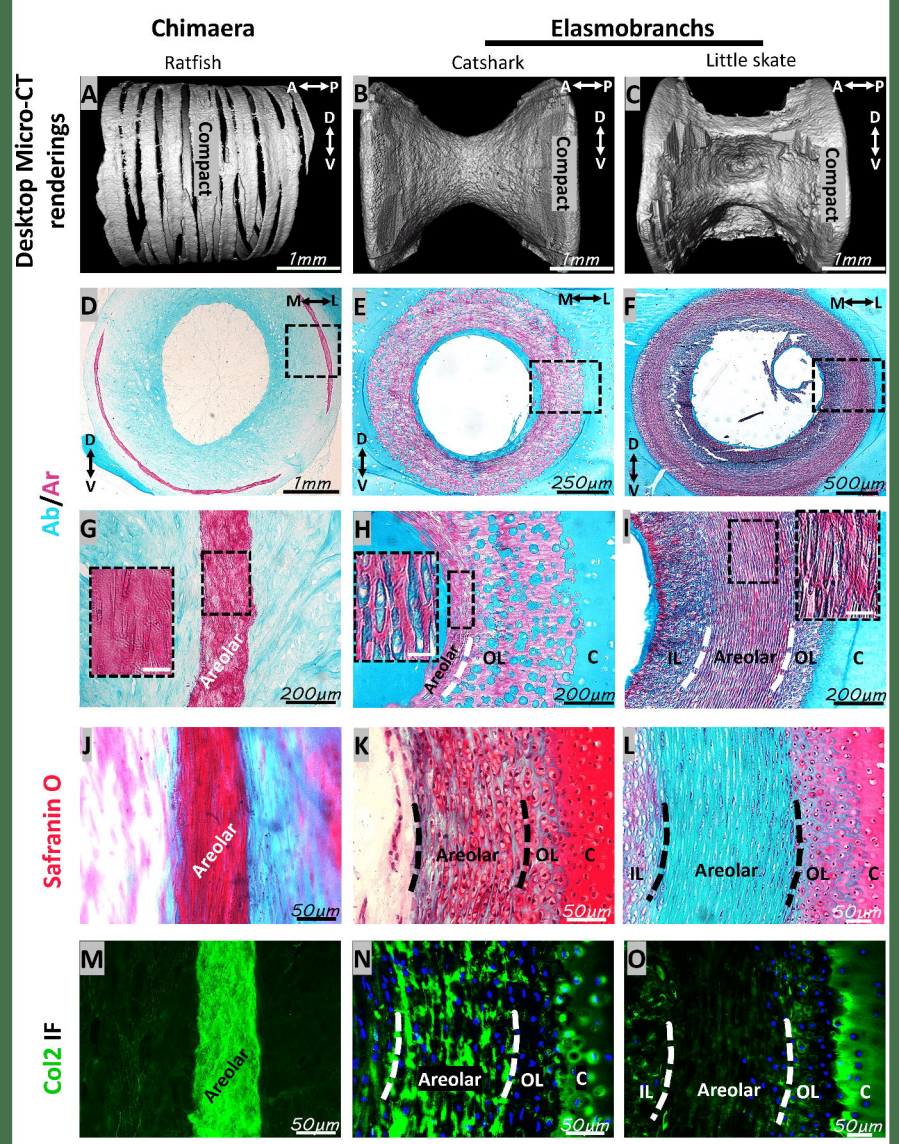
Chimaera
Elasmobranchs
Ratfish
Catshark
Little skate
Desktop Micro-CT renderings
Ab/Ar
Safranin O
Col2 IF
A
B
C
D
E
F
G
H
I
J
K
L
M
N
O
A↔P
D↕V
M↔L
Compact
1mm
250µm
500µm
200µm
50µm
Areolar
OL
C
IL

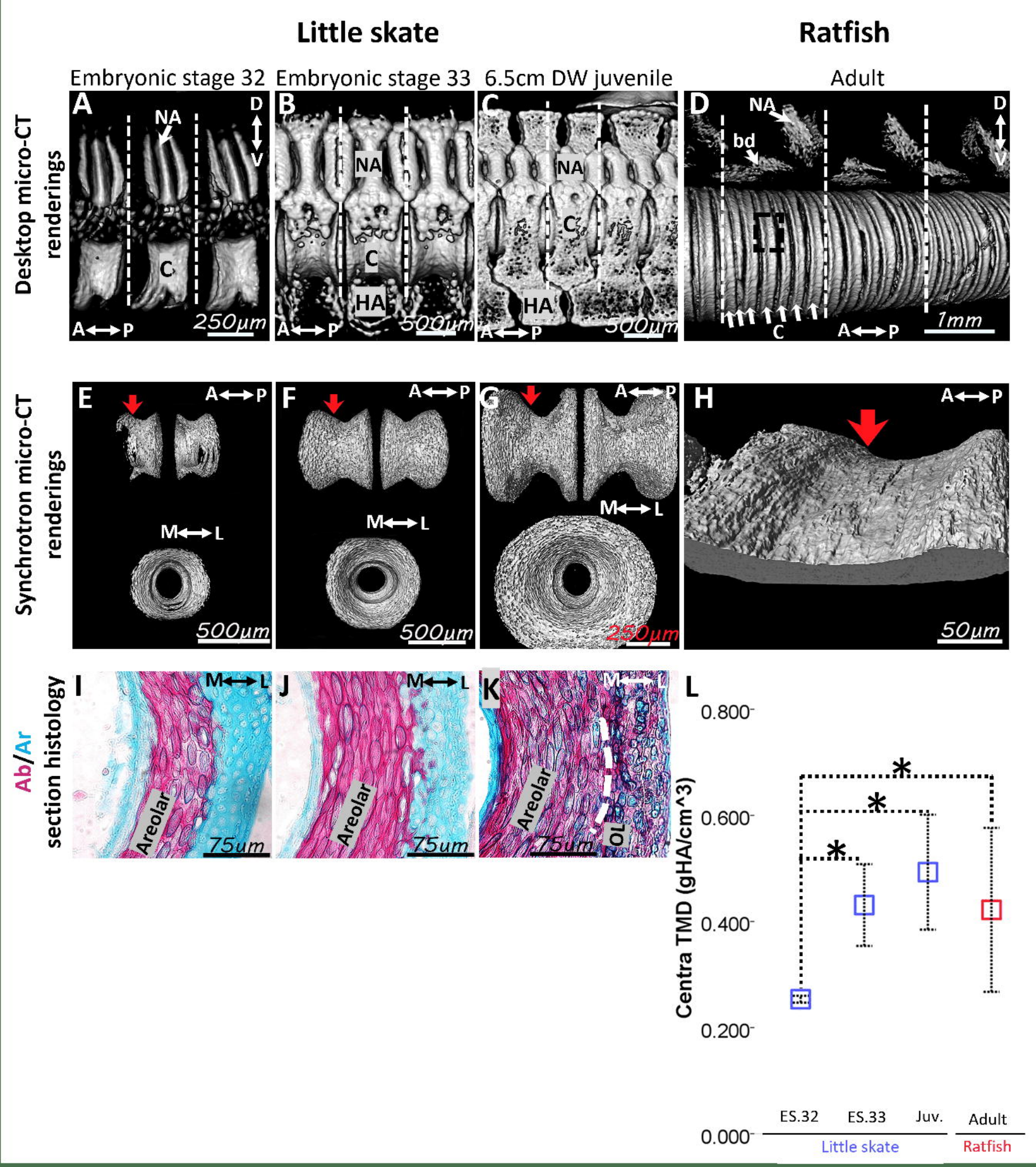
Little skate
Ratfish
Embryonic stage 32
Embryonic stage 33
6.5cm DW juvenile
Adult
Desktop micro-CT renderings
A
NA
D
V
C
A↔P
250µm
B
NA
C
HA
A↔P
500µm
C
NA
C
HA
A↔P
500µm
D
NA
bd
D
V
C
A↔P
1mm
Synchrotron micro-CT renderings
E
A↔P
M↔L
500µm
F
A↔P
M↔L
500µm
G
A↔P
M↔L
250µm
H
A↔P
50µm
Ab/Ar section histology
I
M↔L
Areolar
75um
J
M↔L
Areolar
75um
K
M↔L
Areolar
OL
75um
L
Centra TMD (gHA/cm^3)
0.800
0.600
0.400
0.200
0.000
*
*
*
ES.32
ES.33
Juv.
Adult
Little skate
Ratfish

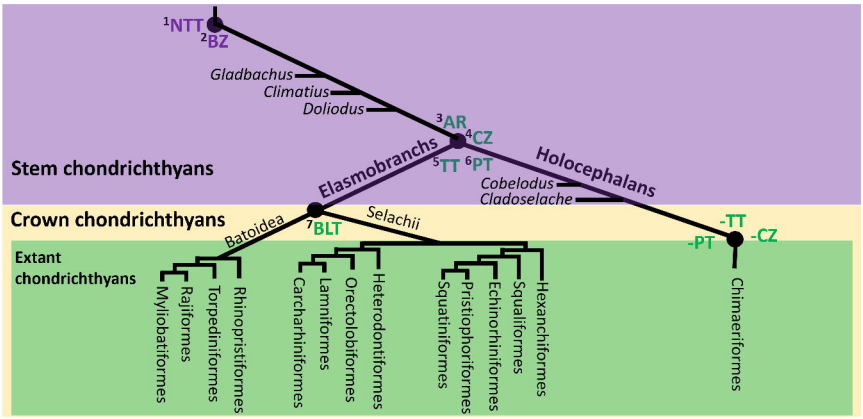

	1	2	3	4	5	6	7
Gladbachus	1	1	0	0	0	0	?
Climatius	1	1	0	0	0	0	?
Doliodus	1	1	0	0	0	0	?
Cobelodus	?	1	?	1	1	1	?
Cladoselache	1	1	?	0	0	0	?
Rhinopristiformes (*P. productus, R. ancylostoma*)	0	1	1	1	1	1	0
Torpediniformes (*Torpedo* sp, *N. bancroftii, T. californica*)	0	1	1	1	1	1	1
Myliobatiformes (*G. micrura, U. halleri, D. sabina, M. californica, R. bonasus*)	0	1	1	1	1	1	0
Rajiformes (*R. clavata, L. erinacea, A. radiata, P. violacea, R. stellulata, R. eglanteria, B. eatonii*)	0	1	1	1	1	1	1
Heterodontiformes (*H. francisci*)	1	1	1	0	0	0	1
Orectolobiformes (*C. punctatum*)	?	1	1	?	?	?	1
Lamniformes (*C. taurus*)	?	1	1	1	1	1	0
Carcharhiniformes (*G.galeus, S. canicula*)	1	1	1	0	0	0	1
(*C. ventriosum*)	?	1	1	0	0	0	1
Squatiniformes (*S. californica*)	0	1	1	1	1	1	0
Squaliformes (*E. spinax, C. crepidater*)	1	1	1	0	0	0	0
(*S. acanthias*)	?	1	1	1	1	1	?
Hexanchiformes (*N. cepedianus*)	?	1	?	0	?	0	?
Chimaeriformes (*H. colliei, C. monstrosa*)	1	1	1	0	0	0	0
(*C. millii*)	?	1	0	0	0	0	?

Derived character

Ancestral character